Numerical Heat Transfer, Part A: Applications: An International Journal of Computation and Methodology
Publication details, including instructions for authors and subscription information:
http://www.tandfonline.com/loi/unht20

EFFECTS OF THERMAL BOUNDARY CONDITION ON BUOYANCY DRIVEN TRANSITIONAL AIR FLOW IN A VERTICAL CYLINDER HEATED FROM BELOW

T. C. Cheng, Y. H. Li, T. F. Lin
[a] National Chiao Tung University
Published online: 29 Oct 2010.

To cite this article: T. C. Cheng, Y. H. Li, T. F. Lin (2000) EFFECTS OF THERMAL BOUNDARY CONDITION ON BUOYANCY DRIVEN TRANSITIONAL AIR FLOW IN A VERTICAL CYLINDER HEATED FROM BELOW, Numerical Heat Transfer, Part A: Applications: An International Journal of Computation and Methodology, 37:8, 917-936

To link to this article: http://dx.doi.org/10.1080/10407780050045892

Numerical Heat Transfer, Part A, 37:917–936, 2000

1040–7782/00 $12.00 + .00

EFFECTS OF THERMAL BOUNDARY CONDITION ON BUOYANCY DRIVEN TRANSITIONAL AIR FLOW IN A VERTICAL CYLINDER HEATED FROM BELOW

T. C. Cheng, Y. H. Li, and T. F. Lin
Department of Mechanical Engineering, National Chiao Tung University, Hsinchu, Taiwan, Republic of China

A three-dimensional unsteady numerical computation was carried out here to investigate the effects of the thermal boundary condition on the convection flow in a vertical, bottom heated cylinder containing air. The thermal condition at the sidewall of the cylinder is assumed to be thermally well insulated or perfectly conducting. Results were obtained for air in a cylinder of finite aspect ratio ($\Gamma = 2$) for various thermal Rayleigh numbers. The predicted results indicate that the flow in the sidewall insulated cylinder is highly asymmetric even at steady state and contains multicellular vortices. The flow formation processes leading to the above structures are relatively complicated. In the early transient two axisymmetric circular vortex rolls, one on top of another, appear. Then the rolls merge asymmetrically. In the late stage the flow deflection by the cylinder top and bottom results in a very complex flow. In the cylinder with a perfectly conducting sidewall the transition from a steady to a time dependent flow is subcritical. However, in the cylinder with an insulated sidewall the flow transition is supercritical.

INTRODUCTION

Buoyancy driven fluid flow in a vertical closed circular cylinder heated from below is known to be rather complex. Only at a slightly supercritical Ra the flow is steady and axisymmetric. A small rise in Ra can cause the flow to become asymmetric and transitional. The unsteady three-dimensional asymmetric flow structure is still poorly understood because of the difficulty in visualizing the flow directly. An initial attempt is made in the present study to investigate how the thermal boundary condition affects the complex flow structure in a vertical cylinder heated from below. To circumvent the difficulties in experimentally observing the flow structures, an unsteady three-dimensional numerical simulation is adopted here to explore the flow.

Suitable models to approximate the thermal buoyancy driven convection in various vertical melt growth configurations for growing bulk crystals have been proposed by Müller, Neumann, and Matz [1]. Meanwhile a model experiment was conducted to visualize the water flow in a cylinder of unit aspect ratio for various thermal conditions covering the steady and unsteady convection. Steady and

Received 9 December 1999; accepted 1 February 2000.
The financial support of this study by the engineering division of National Science Council of Taiwan, R.O.C., through contract NSC83-0401-E-009-009 and National Center for High-Performance Computing is greatly appreciated.
Address correspondence to Professor Tsing-Fa Lin, National Chiao Tung University, Department of Mechanical Engineering, 1001 Ta Hsueh Road, Hsinchu, Taiwan 30010, Republic of China.

NOMENCLATURE

f	oscillation frequency	U, V, W	dimensionless velocity components in the radial, azimuthal, and axial directions
F	Froude number		
g	acceleration due to gravity		
H	height of cylinder	α	thermal diffusivity
k	thermal conductivity	β	volumetric coefficient of thermal expansion
Nu	local Nusselt number		
$\overline{\mathrm{Nu}}_t$	space-average Nusselt number	Γ	aspect ratio, H/D
P	nondimensional pressure	η, ξ	nondimensional coordinates in the radial and axial direction
P_m	modified pressure		
Pr	Prandtl number	υ	kinematic viscosity
r, ϕ, z	coordinates in the radial, azimuthal, and axial directions	ρ	density
		τ_p	nondimensional time period of flow oscillation
Ra	thermal Rayleigh, $g\beta(T_h - T_c)D^3/\alpha\upsilon$	Θ	nondimensional temperature
t, τ	dimensional and dimensionless times		
T	temperature		
T_c	temperature of the cold wall	**Subscripts**	
T_h	temperature of hot wall		
$VC_{\max}$	maximum flow speed at selected cross section	i, j, k	nodes indices
		$\circ$	reference quantity
u, v, w	dimesional velocity components in the radial, azimuthal, and axial directions		

pseudo-steady axisymmetric numerical simulation was carried out by Huang and Hsieh [2] and Lin and Akins [3, 4] to investigate natural convection in a bottom heated vertical cylinder. Both the steady axisymmetric and asymmetric flows were predicted for liquid metal Pr = 0.02 and water (Pr = 6.7) from the three-dimensional numerical simulation by Müller, Neumann, and Weber [5] and Arco and Bontoux [6]. Similar analysis was performed by Neumann [7] for the steady and time-dependent convection. The limits for the appearance of the stable axisymmetric flow were found. The onset of the transient flow oscillation and the induced oscillation frequency also were calculated.

Visualization of the flow of a high Prandtl fluid (silicone oil with Pr = 10^5) in a vertical cylinder heated from below revealed the axisymmetric flow at a slightly supercritical Ra and two distinct three-dimensional flow motions at increasing Ra [8]. Various routes for the transition from the steady laminar flow to the unsteady chaotic flow were determined experimentally from the temperature data by Olson and Rosenberger [9] and Abernathey and Rosenberger [10] for the Xenon gas. Both the Rulle–Taken and period-doubling routes were reported for different ranges of the Ra. Similar experimental study was conducted by Kamotani, Weng, and Ostrach [11] for the gallium melt (Pr = 0.02) for both vertical and inclined cylinders. Based on the temperature data, various convection flow patterns were inferred.

The asymmetric convection in a vertical cylinder was found numerically to result from the lack of the azimuthal symmetry in the imposed wall temperature by Pulicani, Krukowski, Alexander, Ouazzani, and Rosenberger [12]. The critical Ra

for the onset of axisymmetric and nonaxisymmetric thermal convection in a bounded cylindrical layer heated from below and the associated flow patterns were calculated by Charlson and Sani [13–15] based on linear stability analysis. The aspect ratio and thermal state of the sidewall were shown to exert certain influences on the results.

The above literature review clearly indicates that the detailed flow structures driven by the thermal buoyancy in a vertical cylinder remain largely unexplored. More studies are needed to unravel the convection processes in the flow. A three-dimensional unsteady numerical simulation was carried out in the present study to investigate the effects of the lateral wall thermal boundary condition on the detailed flow structures in a bottom heated vertical cylinder.

MATHEMATICAL FORMULATION AND SOLUTION METHOD

Physical Model and Mathematical Formulation

Under consideration is convection of fluid in a bottom heated vertical closed cylindrical box of height H and diameter D, as schematically shown in Figure 1. Initially, at time $t < 0$ the flow is stationary and the temperature is linearly distributed in the vertical direction from the bottom to top walls. At time $t \geq 0$ the bottom wall is maintained at a constant and uniform high temperature T_h and the top wall at a constant and uniform low temperature T_c. The thermal condition at the sidewall of the cylinder is assumed to be thermally well insulated or perfectly conducting. Numerical experiments are to be conducted here to investigate the thermal buoyancy driven flow patterns and their characteristics at steady or statistically stable state for the two different sidewall thermal boundary conditions.

Under the Boussinesq approximation basic nondimensional equations describing the flow and thermal evolution follow:

$$\frac{1}{\eta}\frac{\partial}{\partial \eta}(\eta U) + \frac{1}{\eta}\frac{\partial V}{\partial \phi} + \frac{\partial W}{\partial \xi} = 0 \tag{1}$$

$$\begin{aligned}\frac{\partial U}{\partial \tau} + U\frac{\partial U}{\partial \eta} + \frac{V}{\eta}\frac{\partial U}{\partial \phi} - \frac{V^2}{\eta} + W\frac{\partial U}{\partial \xi} &= -\frac{\partial P}{\partial \eta} \\ &+ \mathrm{Pr}\left\{\frac{\partial}{\partial \eta}\left[\frac{1}{\eta}\frac{\partial}{\partial \eta}(\eta U)\right] + \frac{1}{\eta^2}\frac{\partial^2 U}{\partial \phi^2} - \frac{2}{\eta^2}\frac{\partial V}{\partial \phi} + \frac{\partial^2 U}{\partial \xi^2}\right\} \\ &+ 2\mathrm{Re}_\Omega \mathrm{Pr} V - \mathrm{Ra} F \mathrm{Pr} \Theta \eta\end{aligned} \tag{2}$$

$$\begin{aligned}\frac{\partial V}{\partial \tau} + U\frac{\partial V}{\partial \eta} + \frac{V}{\eta}\frac{\partial V}{\partial \phi} + \frac{UV}{\eta} + W\frac{\partial V}{\partial \xi} &= -\frac{1}{\eta}\frac{\partial P}{\partial \phi} \\ &+ \mathrm{Pr}\left\{\frac{\partial}{\partial \eta}\left[\frac{1}{\eta}\frac{\partial}{\partial \eta}(\eta V)\right] + \frac{1}{\eta^2}\frac{\partial^2 V}{\partial \phi^2} - \frac{2}{\eta^2}\frac{\partial U}{\partial \phi} + \frac{\partial^2 V}{\partial \xi^2}\right\} \\ &- 2\mathrm{Re}_\Omega \mathrm{Pr} U\end{aligned} \tag{3}$$

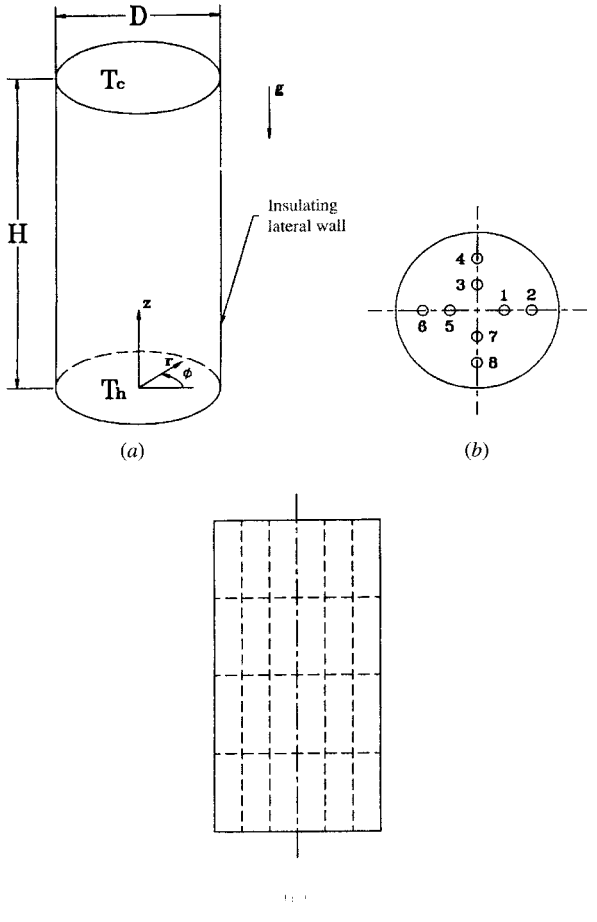

Figure 1. Schematic of (*a*) physical model, (*b*) top view and (*c*) side view of the detection points at all cross sections. Their coordinates follow: 1—(0.5/3, 0, ζ), 2—(1/3, 0, ζ), 3—(0.5/3, π/2, ζ), 4—(1/3, π/2, ζ), 5—(0.5/3, π, ζ), 6—(1/3, π, ζ), 7—(0.5/3, 3π/2, ζ), 8—(1/3, 3π, ζ), where ζ = 0.5, 1.0, 1.5.

$$\frac{\partial W}{\partial \tau} + U\frac{\partial W}{\partial \eta} + \frac{V}{\eta}\frac{\partial W}{\partial \phi} + W\frac{\partial W}{\partial \xi} = -\frac{\partial P}{\partial \xi} + \Pr\left\{\frac{1}{\eta}\frac{\partial}{\partial \eta}\left(\eta\frac{\partial W}{\partial \eta}\right) + \frac{1}{\eta^2}\frac{\partial^2 W}{\partial \phi^2} + \frac{\partial^2 W}{\partial \xi^2}\right\} + \mathrm{Ra}\,\Pr\Theta \tag{4}$$

$$\frac{\partial \Theta}{\partial \tau} + U\frac{\partial \Theta}{\partial \eta} + \frac{V}{\eta}\frac{\partial \Theta}{\partial \phi} + W\frac{\partial \Theta}{\partial \xi} = \frac{1}{\eta}\frac{\partial}{\partial \eta}\left(\eta\frac{\partial \Theta}{\partial \eta}\right) + \frac{1}{\eta^2}\frac{\partial^2 \Theta}{\partial \phi^2} + \frac{\partial^2 \Theta}{\partial \xi^2} \tag{5}$$

subjected to the initial and boundary conditions:

$\tau < 0$

$$U = V = W = \Theta + 0.5 - \left(1 - \frac{\xi}{\Gamma}\right) = 0 \tag{6}$$

$\tau \geq 0$

$$\begin{aligned}
&\xi = 0 && U = V = W = \Theta - 0.5 = 0\\
&\xi = \Gamma && U = V = W = \Theta + 0.5 = 0\\
&\eta = \frac{1}{2} && U = V = W = \frac{\partial \Theta}{\partial \eta} = 0\\
& && (\textit{insulating sidewall})\\
&\eta = \frac{1}{2} && U = V = W = \theta + 0.5 - \left(1 - \frac{\xi}{\Gamma}\right) = 0\\
& && (\textit{conducting sidewall})
\end{aligned} \tag{7}$$

The following nondimensional variables are introduced to nondimensionalize the above flow equations:

$$\begin{aligned}
&\eta = \frac{r}{D} && \phi = \phi && \xi = \frac{z}{D} && U = \frac{u}{\alpha/D}\\
&V = \frac{v}{\alpha/D} && W = \frac{w}{\alpha/D} && P = \frac{P_m}{\rho_0 \cdot \alpha^2/D^2} && \Theta = \frac{T - T_0}{T_h - T_c}\\
&\Gamma = \frac{H}{D} && \Pr = \frac{\upsilon}{\alpha} && \mathrm{Ra} = \frac{g\beta(T_h - T_c)D^3}{\alpha\, v} && \tau = \frac{t}{D^2/\alpha}
\end{aligned} \tag{8}$$

The local Nu for heat transfer from the bottom or top walls of the cylinder to the flow is defined as

$$\mathrm{Nu} = \frac{h_c D}{k} \tag{9}$$

In dimensionless form, it becomes

$$\mathrm{Nu} = -\left.\frac{\partial \Theta}{\partial \xi}\right|_{\xi = 0 \text{ or } \Gamma} \tag{10}$$

The space average Nu is evaluated by the equation

$$\overline{\mathrm{Nu}}_t = \frac{1}{(\pi D^2/4)} \int_0^{D/2} \int_0^{2\pi} \mathrm{Nu} \cdot r \, d\theta \, dr \tag{11}$$

Numerical Scheme and Solution Procedures

After comparing various numerical schemes for the incompressible flow computation, the implicit marker-and-cell (MAC) method developed by Harlow and Welch [16] was chosen to solve the flow equations in primitive form on a staggered grid. In particular, the unsteady terms were treated by the fully implicit first-order Euler approximation and the combined convective and diffusive terms were approximated by the power-law scheme [17]. A uniform grid was employed in the computation. In the η, ϕ, and ξ directions 80, 40, and 60 nodes were placed, respectively. The time interval $\Delta\tau$ was chosen to be 10^{-4}.

In a cylindrical domain encountered here singularity of the basic flow equations at the cylinder axis ($\eta = 0$) needs to be overcome. This singularity is avoided by placing the temperature node at $\eta = 0$ in the staggered grid instead of the velocity components. Then the energy equation is integrated over a control volume for this temperature node. The divergence theorem [18] is used to transform the volume integral into a surface integral. Thus the combined conductive and convective energy flux needs to be evaluated only at the control surface that surrounds the cylinder axis, and the singularity is prevented.

Computation was started from the initiation of the transient to the final steady state or to the statistical state when the flow does not become steady for a long time. The convergence criteria for the U, V, W, P, and Θ at each time step were

$$\frac{\Sigma_{i,j,k} \left| \zeta_{i,j,k}^{m+1} - \zeta_{i,j,k}^{m} \right|}{\max \left| \zeta^{m+1} \right| ((I \cdot J + 1) \cdot K)} < 10^{-3} \tag{12}$$

where I, J, and K, respectively, are the total numbers of nodes in the η, ϕ, and ξ directions, and ζ^{m+1} denotes U, V, W, P, or ϕ at the $(m+1)$th iteration. Moreover, the flow is considered to have reached steady state when the relative differences in ζ between two consecutive time steps are below 10^{-6}.

Verification of Numerical Scheme

Since no analytical solution is available for the three-dimensional natural convection in a confined box, it is necessary to compare our results with the published data in the literature to insure the accuracy of the proposed solution

method. The predicted steady flow structure for a vertical cylinder heated from below with an insulated sidewall for Pr = 6.7, Ra = 22,400, and $\Gamma = 0.5$ was compared with that of Müller et al. [5]. The agreement was good. Sampled results from the grid-independence test for the steady temperature and velocity distributions in the sidewall-conducting cylinder ($\Gamma = 2$) for Pr = 0.7 and Ra = 30,000 for four different grids 80*40*60, 100*40*60, 80*64*60, and 80*40*80 with $\Delta\tau = 10^{-4}$ were compared. The agreement also was good. Further sampled results for the time variations of temperature and velocity in the sidewall insulated cylinder for a time periodic case for Ra = 90,000 computed again from the same four different grids at $\Delta\tau = 10^{-4}$ were compared. The agreement was relatively good. The other sampled results for the time variations of temperature and velocity in the sidewall-conducting cylinder again for the time periodic case at Ra = 62,000 computed for the spatial grid 80*40*60 at three time intervals $\Delta\tau = 1.0*10^{-4}$, $7.5*10^{-5}$, and $5.0*10^{-5}$ were compared. The agreement also was relatively good. Through these program tests the solution method is considered to be suitable for the present problem.

RESULTS AND DISCUSSION

To illustrate the effects of the sidewall thermal condition on the buoyancy driven flow structures in a vertical closed cylinder, computations were carried out specifically for air flow Pr = 0.7 in a sidewall-insulated or conducting cylinder of finite aspect ratio ($\Gamma = 2$) with Ra ranging from 20,000 to 100,000. The results from these computations showed that in the sidewall-insulated cylinder the flow eventually evolves to a steady state but is highly asymmetric for Ra $\leq$ 40,000. As the Ra is in the range of 45,000 to 90,000, the flow was found to evolve gradually to time periodic state. Beyond that the flow begins to show chaotic oscillation in time. These results suggest that the buoyancy induced flow transition is supercritical. The results for the sidewall-conducting cylinder, however, indicated that the driven flow remains steady for Ra up to 61,000. For a very small increase of Ra to 62,000 the flow evolves to a time periodic state. But the time periodic flow only exists in a very narrow Ra range, and beyond 63,000 the flow oscillates chaotically in time. Hence the buoyancy driven flow in a sidewall-conducting cylinder experiences a subcritical transition. In the following, the detailed flow patterns at steady and time periodic states for the two sidewall thermal conditions will be examined in detail.

Steady Flow Structures

The transient flow structures during the flow formation leading to the final steady flow at low Ra are examined first. To illustrate the typical time evolution of the flow structure at a low thermal buoyancy, Figure 2 presents the predicted three-dimensional velocity vector maps and isotherms at selected vertical planes at various instants from the initiation of the transient to the final steady state for Ra = 20,000 for the sidewall-insulated cylinder. The results indicate that immediately after the transient is started, a weak axisymmetric flow is induced in the cylinder (Figure 2*a*). Specifically, the flow consists of two horizontal circular vortex

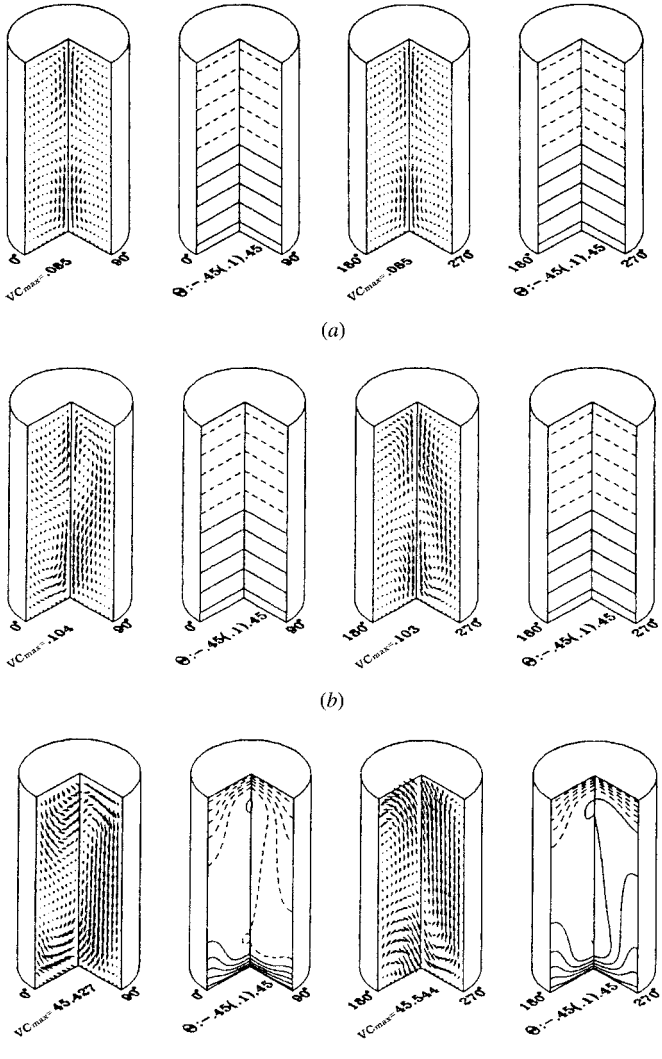

Figure 2. Three-dimensional velocity vectors and isotherms at selected vertical planes at various selected time instants from the initiation of the transient to the final steady state for $Pr = 0.7$, $\Gamma = 2$, and $Ra = 20{,}000$. (*a*) $\tau = 1$; (*b*) $\tau = 1.35$; and (*c*) steady state ($\tau > 9$).

rolls of similar size (like torus), one on top of the other. In the upper vortex roll the flow rises near the cylinder axis and sinks near the sidewall. The circulation is in the opposite direction in the lower roll. In this weak vortex flow a nearly linear vertical temperature distribution still prevails, implying that heat transfer in the flow is conduction dominated. Note that slightly later at $\tau = 1.35$ (Figure 2*b*), the two vortex rolls break around the planes $\phi = 90°$ and 270° near the midheight of the cylinder and merge together. The flow is no longer axisymmetric. Then the circulation cells near the plane $\phi = 0°$ and 180° also merge together. As time increases, the flow strengthens slowly and has a noticeable circumferential component. It is interesting to notice that as $\tau > 1.50$, the flow is accelerated quickly by the buoyancy with the VC_{max} increased from 0.198 at $\tau = 1.50$ to 29.52 at $\tau = 2.0$. The associated isotherms suggest that convection is the dominant heat transfer mode. The flow then gradually approaches steady state (Figure 2*c*) for $\tau > 9.0$. Even at this low Ra the induced steady flow is highly asymmetric and contains highly distorted vortices. More specifically, the steady flow consists of a main recirculation sinking along the sidewall around the plane $\phi = 90°$ and rising along the opposite sidewall near the plane $\phi = 270°$. This recirculation is highly distorted with the flow near the sidewall at the plane $\phi = 0°$ and 180°, respectively, ascending in the bottom half of the cylinder and descending in the top half. A closer inspection of the flow reveals that the downward flow along the sidewall near $\phi = 90°$ also can be deflected laterally toward $\phi = 0°$ and 180° when hitting the bottom wall, in addition to directly reversing its direction to move up along the sidewall near $\phi = 270°$. Thus near $\phi = 0°$ and 180° the flows in the top and bottom halves of the cylinder are in the opposite directions. At a slightly higher buoyancy of Ra = 30,000 the evolution of the flow structure resembles that presented above for Ra = 20,000.

Similar flow evolution is noted in the sidewall-conducting cylinder by comparing the results in Figures 2 and 3 for the two cylinders at Ra = 20,000. A close inspection of these results, however, reveals that for the perfectly conducting sidewall the buoyancy driven flow is weaker and in a slower evolution.

It is of interest to note that at a slightly higher buoyancy the driven flow is significantly stronger in the sidewall-conducting cylinder, as evident from the results in Figures 4 and 5 for the two cylinders for Ra = 35,000.

As the Ra is raised further to 45,000, the flow in the sidewall-insulated cylinder gradually becomes time periodic. But in the sidewall-conducting cylinder the flow remains steady for Ra up to 61,000. The flow evolves to a time periodic state for Ra = 62,000. Note that the change in the flow structure in the sidewall-conducting cylinder is only slight when Ra is raised from a low level for the steady flow to a high level for the time dependent flow.

Time Periodic Flow Structures

The change in the flow structure in a typical time periodic state for Ra = 45,000 is illustrated in Figure 6 for the sidewall-insulated cylinder. In this figure τ denotes a certain time instant when the flow has already evolved to the time periodic state. Note that in a periodic cycle there is only a slight change in the flow structure with time. However, substantial velocity and temperature oscillations with

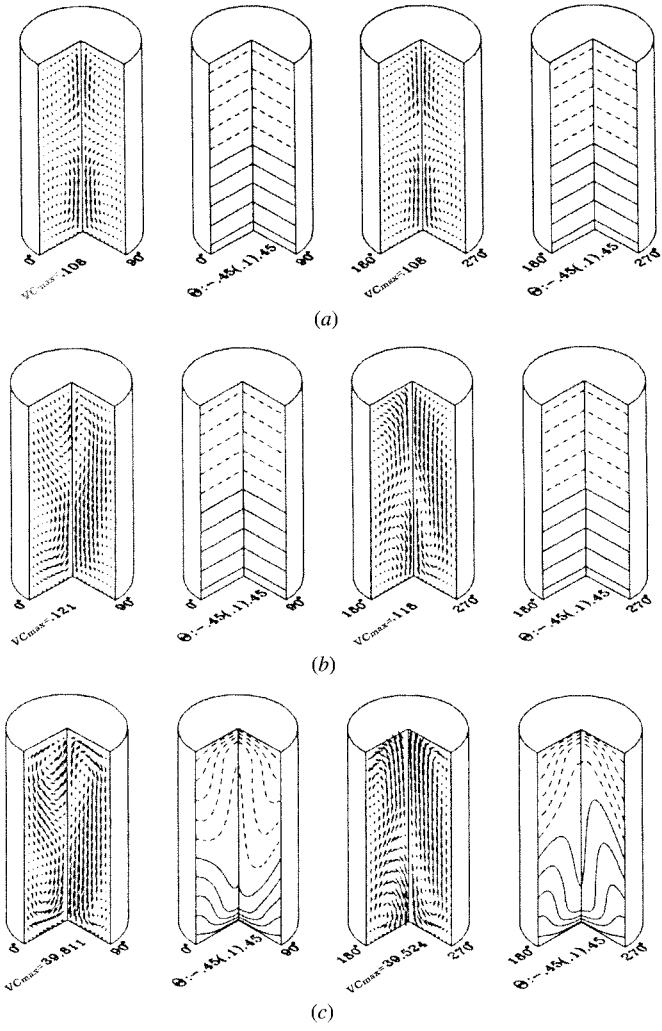

Figure 3. Three-dimensional velocity vectors and isotherms at selected vertical planes at selected time instants from the initiation of the transient to the final steady state for Pr = 0.7, $\Gamma = 2$, and Ra = 20,000 in the sidewall-conducting cylinder. (*a*) $\tau = 2$; (*b*) $\tau = 2.4$; (*c*) steady state ($\tau > 12$).

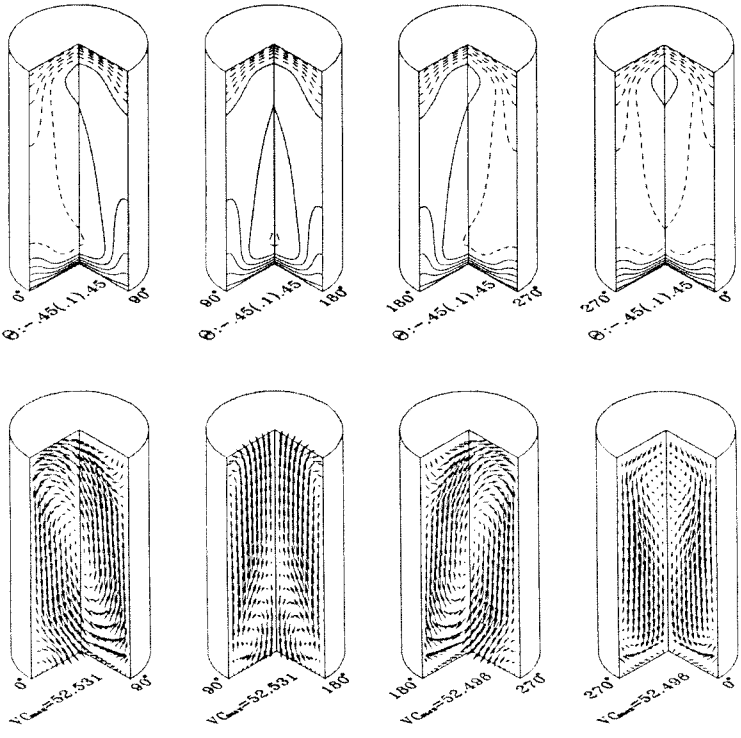

Figure 4. Steady three-dimensional velocity vectors and isotherms at selected vertical planes for Pr = 0.7, $\Gamma = 2$, and Ra = 35,000 in the sidewall-insulated cylinder.

time result. Besides, the entire flow oscillates at a single fundamental frequency $f_1 = 2.288$ and its harmonics. Also it is noted that the oscillation amplitudes of the temperature and velocity depend significantly on the locations.

For a further raise of the Ra to 55,000 the resulting flow in the sidewall-insulated cylinder strengthens slightly and also oscillates periodically in time at a slightly higher fundamental frequency $f_1 = 2.353$. In addition, the flow structure is in a larger distortion. Obviously, the harmonics are slightly stronger than those at Ra = 45,000. Thus the flow structure is more complex. Also there is a significant velocity oscillation with time. Besides, the main flow recirculation also moves slowly up and down with time. The associated time variation of the temperature field also is large. At still higher Ra of 60,000 and 65,000 the induced flow also oscillates at a single fundamental frequency with $f_1 = 2.421$ for Ra = 60,000 and $f_1 = 2.469$ for Ra = 65,000.

Now as the Ra is raised from 65,000 to 70,000, a significant change in the flow structure occurs in the sidewall-insulated cylinder. More specifically, the three-dimensional velocity and temperature fields in a periodic cycle shown in Figure 7

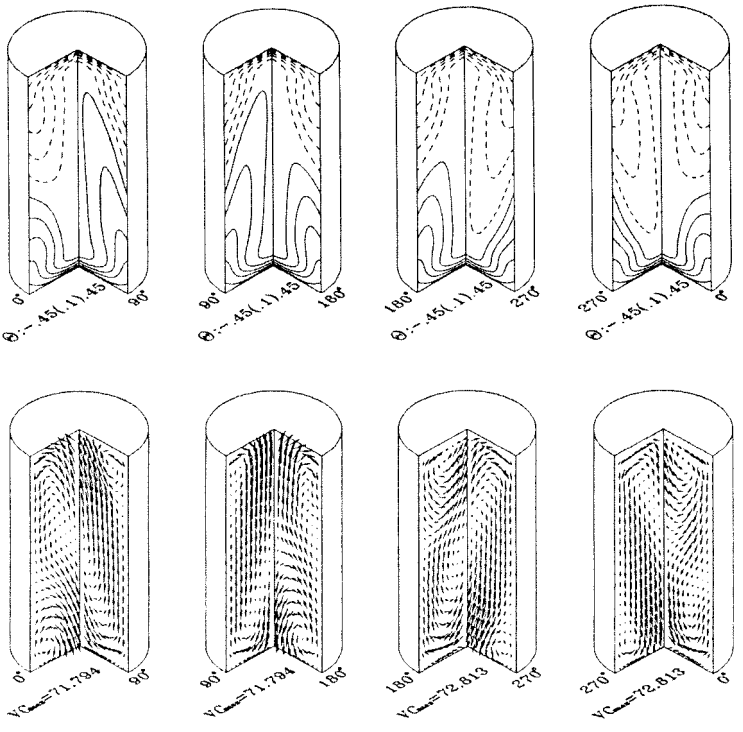

Figure 5. Steady three-dimensional velocity vectors and isotherms at selected vertical planes for Pr = 0.7, $\Gamma = 2$, and Ra = 35,000 in the sidewall-conducting cylinder.

indicate that the flow ascends along the sidewall around the plane $\phi = 270°$ and descends near the plane at $\phi = 90°$ at time τ. A small vortice is induced near the plane $\phi = 270°$ in the bottom half of the cylinder and another vortice near the plane $\phi = 90°$ in the top half of the cylinder. In addition, around the planes $\phi = 0°$ and 180° two vortices are present. As time proceeds, the small upper cells grow and slowly move downward in the first half of the periodic cycle. Then in second half of the cycle, reverse processes take place to restore the flow to the original state at τ. At still higher Ra of 75,000 and 85,000 the induced flows are still time periodic and are qualitatively similar to that for Ra = 70,000. Note that when Ra = 85,000, the flow structure "resembles" that at Ra = 75,000 but is a "mirror image." The induced flows in these two cases circulate in opposite directions. As the Ra is further raised to 90,000, the flow structure is in an even larger distortion. The up and down moving and growth and decay of the vortices are much stronger for increasing Ra. For a further raise of the Ra to 95,000 and 100,000, the flow becomes chaotic in time and the corresponding flow structures are rather complex.

It was mentioned above that as the Ra was raised to 62,000, the flow in the sidewall-conducting cylinder was found to evolve gradually to a time periodic state.

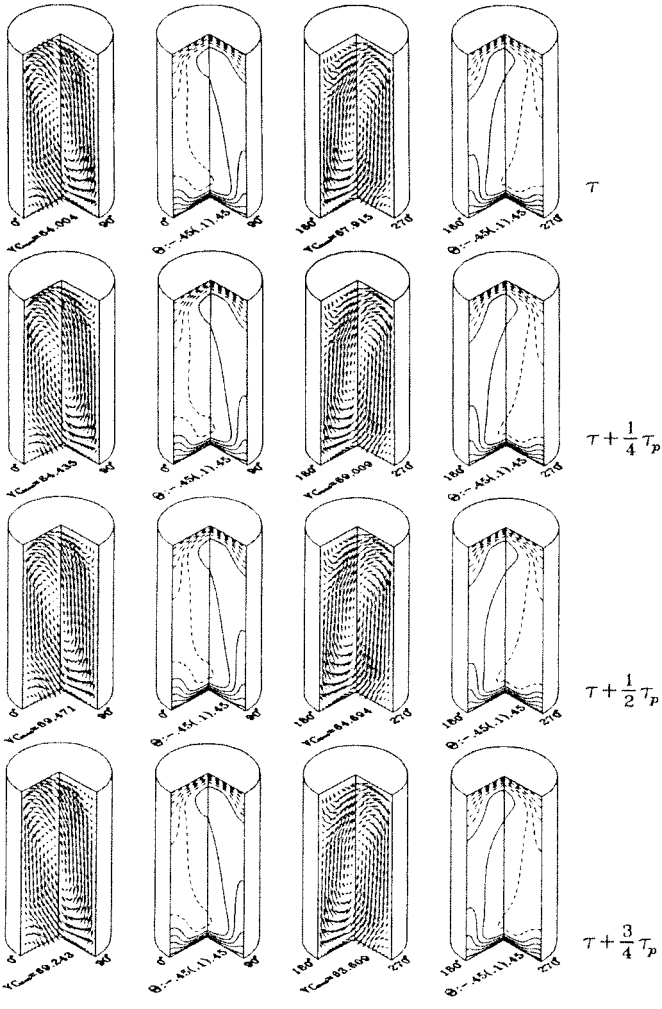

Figure 6. Three-dimensional velocity vectors and isotherms at selected vertical planes at four selected time instants in a periodic cycle for $\mathrm{Pr} = 0.7$, $\Gamma = 2$, and $\mathrm{Ra} = 45{,}000$ in the sidewall-insulated cylinder ($\tau_p = 0.437$).

A closer inspection of the time periodic flow for $\mathrm{Ra} = 62{,}000$ in Figure 8 reveals that the main flow recirculation moves slightly up and down with time. The change of the temperature contours with time is rather substantial in this time periodic flow. The computed results for higher Ra showed that the time periodic flow only exists in a very narrow range of the Ra. Specifically, a small increase of the Ra to 63,000 causes the flow to evolve to a chaotic state. This chaotic state prevails for $\mathrm{Ra} \geq 63{,}000$. These results suggest that the transition from the steady to time dependent states is subcritical in the cylinder with a perfectly conducting sidewall.

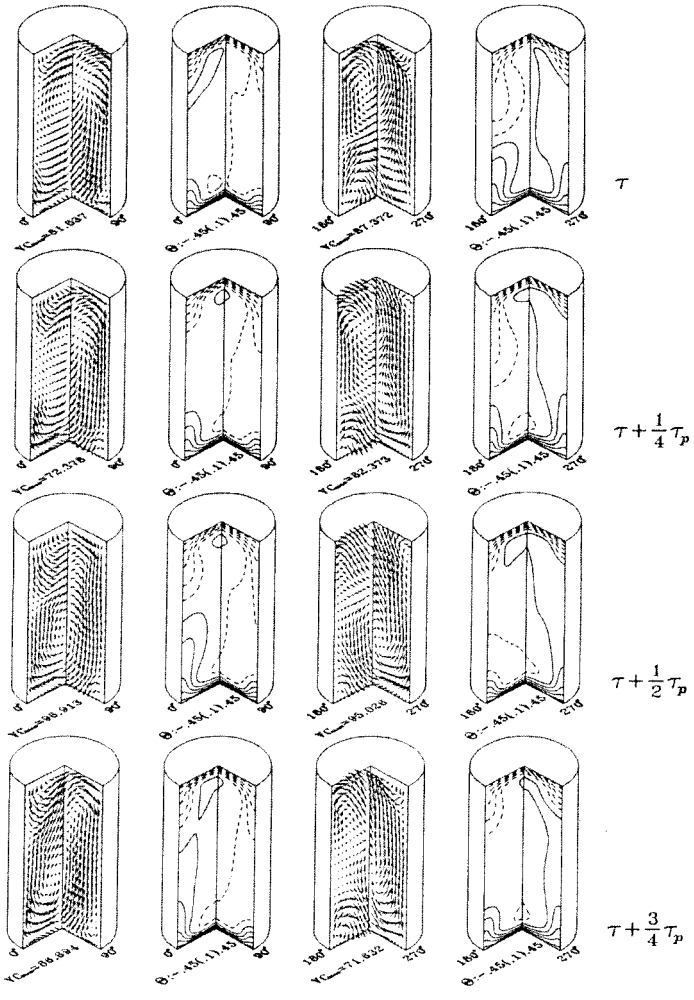

Figure 7. Three-dimensional velocity vectors and isotherms at selected vertical planes at four selected time instants in a periodic cycle for $Pr = 0.7$, $\Gamma = 2$, and $Ra = 70{,}000$ in the sidewall-insulated cylinder ($\tau_p = 0.395$).

Nusselt Number

To further illustrate the heat transfer in the cylinders, the local Nu distributions at the top wall are examined. The steady Nu distributions at the top wall shown in Figures 9 and 10 for the steady flow in the two cylinders indicate that the contours are highly asymmetric in the sidewall-insulated cylinder. But in the sidewall-conducting cylinder they are nearly axisymmetric. Figure 11 presents the local Nu distributions in the sidewall-insulated cylinder at four selected time

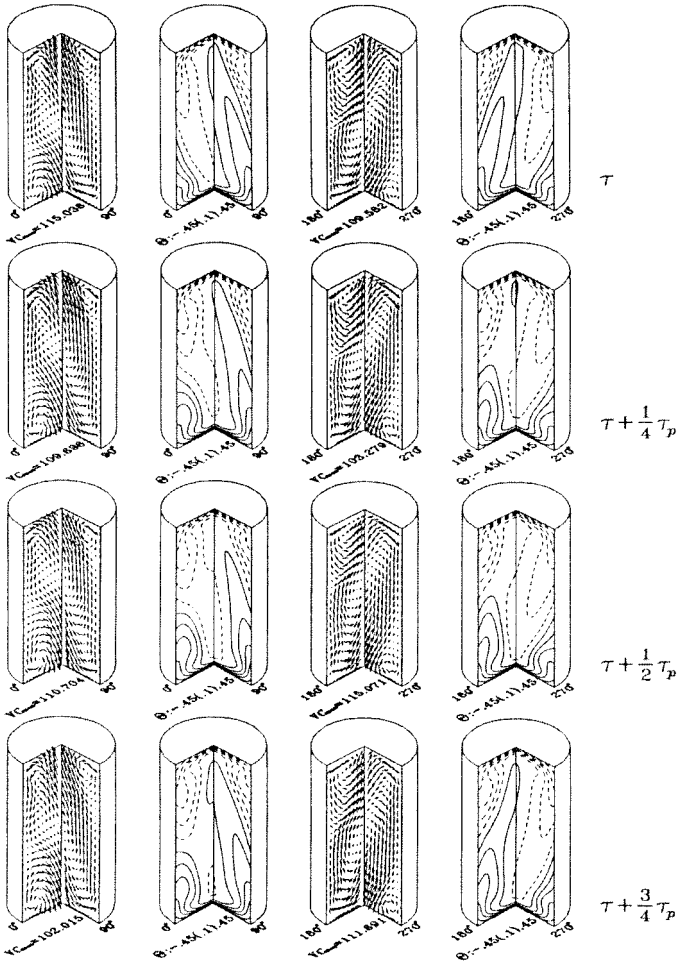

Figure 8. Three-dimensional velocity vectors and isotherms at selected vertical planes at four selected time instants in a periodic cycle for Pr = 0.7, $\Gamma = 2$, and Ra = 62,000 in the sidewall-conducting cylinder ($\tau_p = 0.812$).

instants in a periodic cycle and the corresponding space-average Nu variation with time for Ra = 55,000. The results indicate that the Nu contours rotate circumferentially with time and are similar in shape to that for Ra = 40,000 (Figure 9*c*). The oscillation amplitude of $\overline{\mathrm{Nu}}_t$ is small. The results for higher Ra of 70,000 and 90,000 indicated that the oscillation amplitudes of the space-average Nusselt number $\overline{\mathrm{Nu}}_t$ and the local Nu were obviously larger for higher Ra.

The corresponding time periodic, local Nu distributions at the top wall in the sidewall-conducting cylinder and the $\overline{\mathrm{Nu}}_t$ variation with time presented in Figure

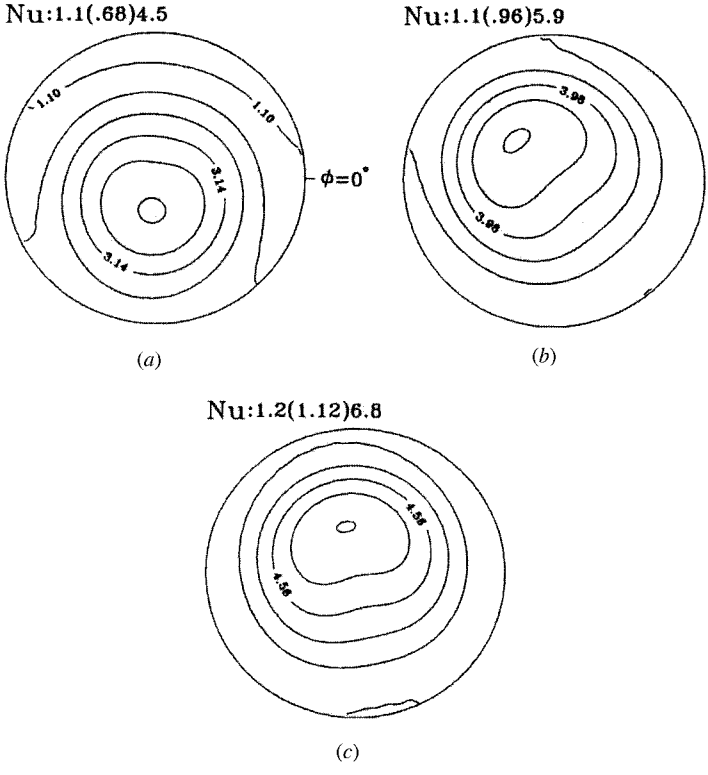

Figure 9. Steady local Nu distributions for (*a*) Ra = 20,000; (*b*) Ra = 35,000; and (*c*) Ra = 40,000 for Pr = 0.7 and $\Gamma = 2$.

12 for Ra = 62,000 indicate that the Nu values and $\overline{\mathrm{Nu}}_t$ vary significantly with time. At Ra = 100,000, the flow is chaotic. The associated local Nu distributions indicate that the peak Nu value and the location where it appears vary substantially with time and the contours are somewhat distorted.

CONCLUDING REMARKS

Based on the results from the present transient three-dimensional numerical simulation, the buoyancy driven flow in the cylinder with its sidewall perfectly conducting remains steady for a much wider range of Ra. However, the time periodic flow prevails only in a very narrow range of the Ra. Thus the transition from a steady to a time dependent flow is subcritical. But in the cylinder with an insulated sidewall the time periodic flow exists in a wide range of the Ra, and the flow transition is supercritical. Moreover, the flow is highly asymmetric and contains multicellular vortices. At time periodic and chaotic states the growth and decay and the downward and upward motion of the vortices increase with the Ra.

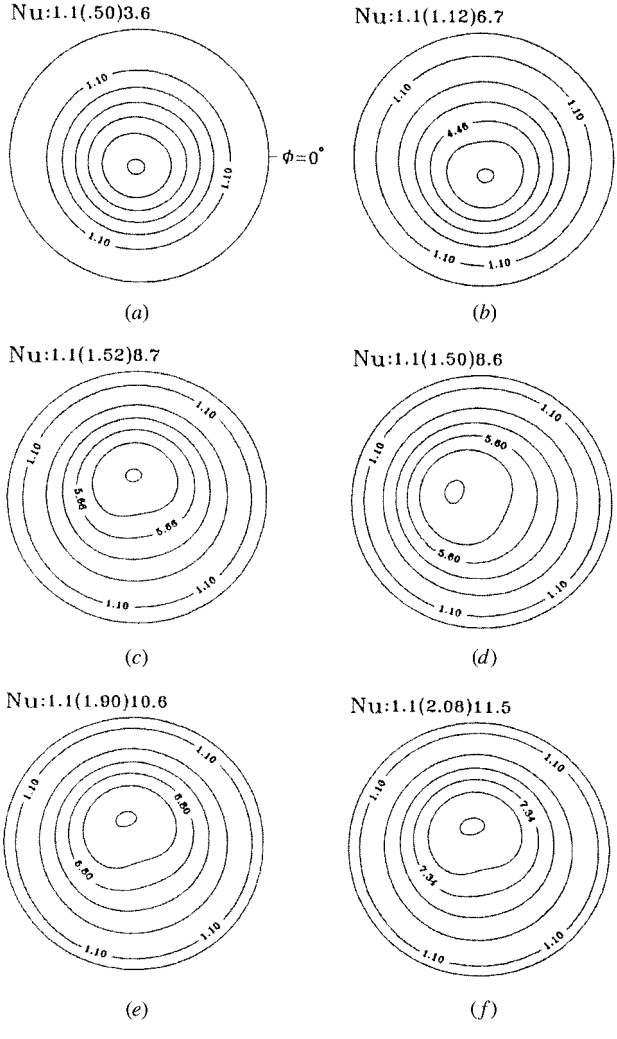

Figure 10. Steady local Nu distributions for (*a*) Ra = 20,000; (*b*) Ra = 30,000, (*c*) Ra = 40,000, (*d*) Ra = 50,000, (*e*) Ra = 55,000, and (*f*) Ra = 61,000 for Pr = 0.7 and $\Gamma = 2$ in the sidewall-conducting cylinder.

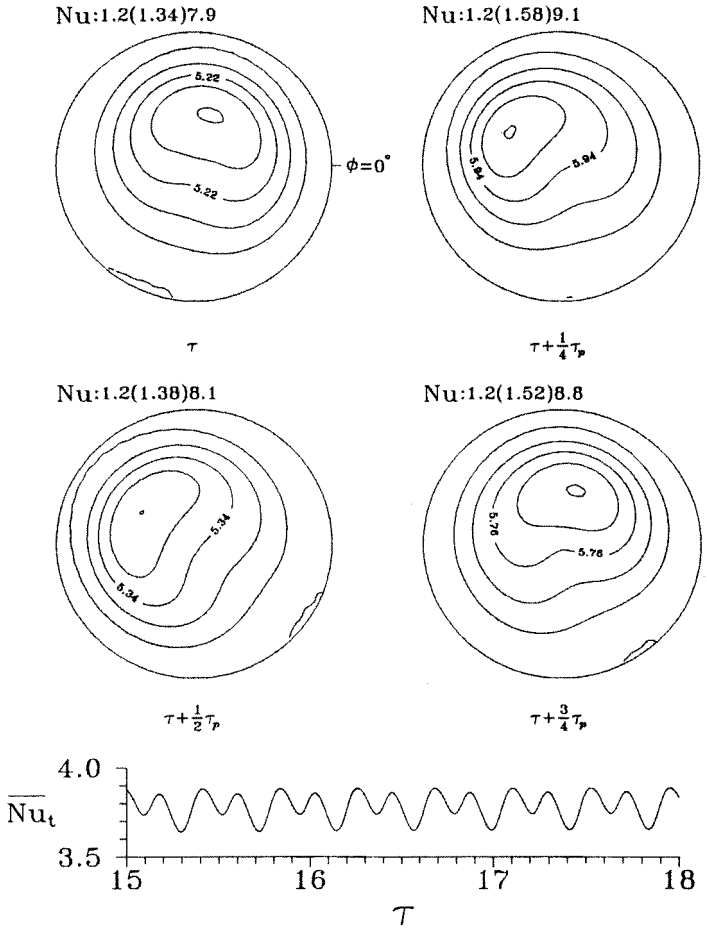

Figure 11. Local Nu distributions at four selected time instants in a periodic cycle and the space-average Nu variation with time for Pr = 0.7, Γ = 2, and Ra = 55,000 (τ_p = 0.425).

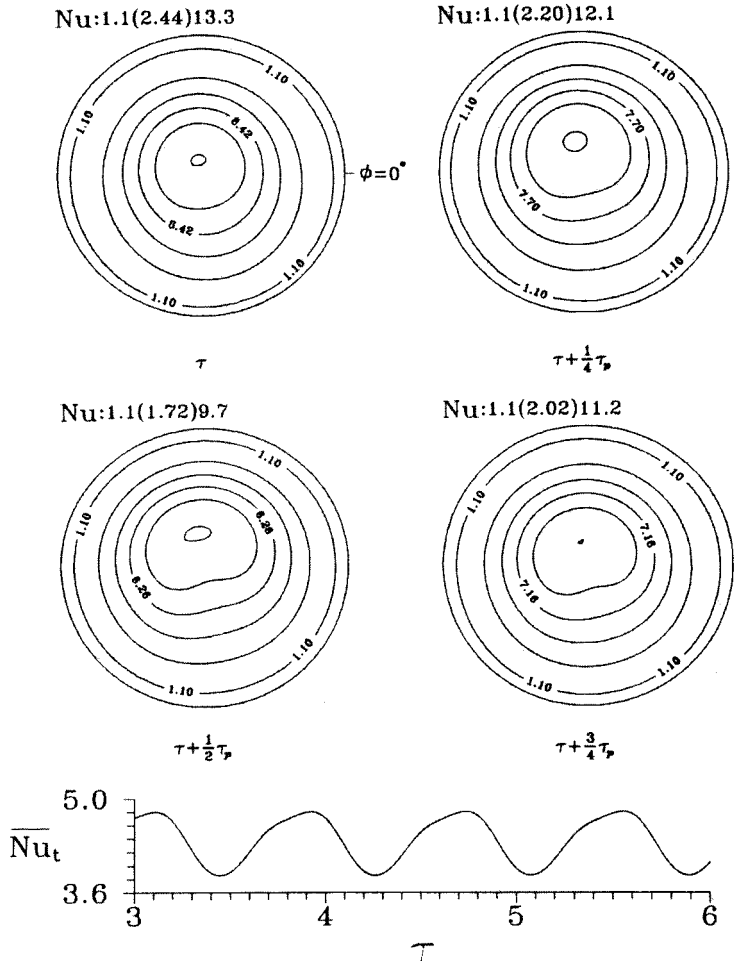

Figure 12. Local Nu distributions at four selected time instants in a periodic cycle and the space-average Nu variation with time for Pr = 0.7, Γ = 2, and Ra = 55,000 in the sidewall-conducting cylinder ($\tau_p = 0.425$).

REFERENCES

1. G. Müller, G. Neumann, and H. Matz, A Two-Rayleigh-Number Model of Buoyancy-Driven Convection in Vertical Melt Growth Configurations, *J. Crystal Growth*, vol. 84, pp. 36–49, 1987.
2. D. Y. Huang and S. S. Hsieh, Analysis of Natural Convection in a Cylinder Enclosure, *Numerical Heat Transfer*, vol. 12, pp. 121–135, 1987.
3. Y. S. Lin and R. G. Akins, Pseudo-Steady-State Natural Convection Heat Transfer Inside a Vertical Cylinder, *ASME J. Heat Transfer*, vol. 108, pp. 310–316, 1986.
4. Y. S. Lin and R. G. Akins, Thermal Description of Pseudosteady-State Natural Convection Inside a Vertical Cylinder, *Int. J. Heat Mass Transfer*, vol. 29, pp. 301–307, 1986.

5. G. Müller, G. Neumann, and W. Weber, Natural Convection in Vertical Bridgman Configurations, *J. Crystal Growth*, vol. 70, pp. 78–93, 1984.
6. E. C. Arco and P. Bontoux, Numerical Solution and Analysis of Asymmetric Convection in a Vertical Cylinder: An Effect of Prandtl Number, *Phys. Fluids A*, vol. 1, no. 8, pp. 1348–1359, 1989.
7. G. Neumann, Three-Dimensional Numerical Simulation of Buoyancy-Driven Convection in Vertical Cylinders Heated from Below, *J. Fluid Mech.*, vol. 214, pp. 559–578, 1990.
8. R. S. Figliola, Convection Transitions Within a Vertical Cylinder Heated from Below, *Phys. Fluids*, vol. 29, no. 7, pp. 2028–2031, 1986.
9. J. M. Olson and F. Rosenberger, Convective Instabilities in a Closed Vertical Cylinder Heated from Below. Part 1. Monocomponent Gases, *J. Fluid Mech.*, vol. 92, pp. 609–629, 1979.
10. J. R. Abernathey and F. Rosenberger, Time-Dependent Convective Instabilities in a Closed Vertical Cylinder Heated from Below, *J. Fluid Mech.*, vol. 160, pp. 137–154, 1985.
11. Y. Kamotani, F. B. Weng, and S. Ostrach, Oscillatory Natural Convection of a Liquid Metal in Circular Cylinders, *ASME J. of Heat Transfer*, vol. 116, pp. 627–632, 1994.
12. J. P. Pulicani, S. Krukowski, J. I. D. Alexander, J. Ouazzani, and F. Rosenberger, Convection in an Asymmetrically Heated Cylinder, *Int. J. Heat Mass Transfer*, vol. 35, pp. 2119–2130, 1992.
13. G. S. Charlson and R. L. Sani, Thermoconvective Instability in a Bounded Cylindrical Fluid Layer, *Int. J. Heat Transfer*, vol. 13, pp. 1479–1496, 1970.
14. G. S. Charlson and R. L. Sani, On Thermoconvective Instability in a Bounded Cylindrical Fluid Layer, *Int. J. Heat Transfer*, vol. 14, pp. 2157–2160, 1971.
15. G. S. Charlson and R. L. Sani, Finite Amplitude Axisymmetric Thermoconvective Flows in a Bounded Cylindrical Layer of Fluid, *J. Fluid Mech.*, *Part* 2, vol. 71, pp. 209–229, 1975.
16. F. H. Harlow and J. E. Welch, Numerical Calculation of Time-Dependent Viscous Incompressible Flow of Fluid with Free Surface, *Phys. Fluids*, vol. 8, pp. 2182–2189, 1965.
17. S. V. Patankar, *Numerical Heat Transfer and Fluid Flow*, Chap. 5, Hemisphere, Washington, DC, 1980.
18. E. Haung and K. K. Choi, *Method of Engineering Mathematics*, p. 237, Prentice-Hall, Englewood Cliffs, NJ, 1993.